1R.6 AIRBORNE DUAL-DOPPLER RADAR OBSERVATIONS OF HORIZONTAL VELOCITY FIELDS IN GROWING CUMULUS

Rick Damiani*, Gabor Vali, and Samuel Haimov
Department of Atmospheric Science, University of Wyoming

1. INTRODUCTION

In this paper, we concentrate on the kinematic aspects of summer continental cumuli, extending the view offered in Damiani et al. (2005) (henceforth DVH05), where a conceptual model of shallow to mid-size cumulus growth, based on airborne vertical plane dual-Doppler observations and in situ records, is described. In DVH05, the authors portray the clouds, in their formative stages, as the result of *multi-thermal* or *multi-bubble* entities forming and intruding the clouds. The pulsating nature of clouds influences both the spatial arrangement of updrafts and downdrafts as well as the hydrometeor spatial distribution. A vortex-ring type of motion was detected in the thermals. This mechanics has a number of consequences from the purely fluid-dynamical aspects of the evolution and lifespan of the bubble, to an increased residence time of the small droplets carried aloft by the updraft, from ambient air entrapment at the base of the thermal, to the recycling of precipitation-size hydrometeors from the sides into the thermal core with implications on the precipitation generation rate. This emerging picture is in agreement with the studies and models proposed by Blyth et al. (1988); Blyth (1993); Carpenter et al. (1998); Zhao and Austin (2005) and tank experiment results by Scorer and Ludlam (1953); Scorer (1957); Woodward (1959); Sanchez et al. (1989); Johari (1992); Morton (1997), and provides further clarifications.

In this paper, kinematic patterns and vortical structures in horizontal planes are discussed in an effort to complete the above model of cumulus growth, tying them to those in vertical planes. Horizontal air motion in shallow cumulus convection has received little attention from meteorologists, even though its importance may be evinced from fine-scale observations (e.g., DVH05). Because it influences the lifetime and evolution of the clouds, and it affects the cloud microphysics via entrainment processes, the horizontal motion field plays a relevant role within shallow cumulus convection. The main hurdle in its study has been the lack of appropriate observational tools.

For this study, we employed the high-spatial resolution, sensitivity, mobility and dual-Doppler capabilities of the Wyoming Cloud Radar (WCR): a 3.2 mm wavelength (95 GHz) Doppler radar mounted on the University of Wyoming KingAir research aircraft (UWKA) (Pazmany et al. 1994; Damiani and Haimov 2005a). The four available radar antennas provide for the capability of switching between different dual-beam configurations; among those, two allow for the 2-D velocity field retrieval from the analysis of two independent radial velocity components. In this study, the HBDD (Horizontal Beam dual-Doppler) configuration, utilizing the two antennas scanning a horizontal plane starboard of the aircraft, was extensively employed. In situ thermodynamic and microphysical data complement the radar pictures to focus on and to extend the dynamical model of thermal in cumuli. For a description of the instrumental suite on-board the UWKA refer to DVH05. The data were collected during the second phase of the *'High Plains Cumulus Experiment'* (HiCu03) campaign in the summer of 2003 over Southeastern Wyoming (DVH05).

In Section 2, the WCR/UWKA radar installation is briefly presented together with a summary of the technique adopted to retrieve the two-dimensional kinematic fields from the dual-Doppler data.

Section 3 presents the typical environment in which the continental cumuli were investigated and their basic properties derivable from single Doppler radar and in situ data.

Section 4 reports case studies demonstrating the characteristic length scales and gradients in the horizontal plane and evidence of vertical vorticity structures.

Section 5 discusses the main findings within the broader picture of a cumulus growth model with connections between the horizontal and vertical dynamics. A mechanism for the generation of vertical vorticity is identified in agreement with aerodynamic models and available data. Section 6 reports a summary of the results.

2. THE WYOMING CLOUD RADAR HBDD SET-UP

The WCR is a 95 GHz multi-fixed-beam Doppler radar typically on board the UWKA research aircraft. A detailed description of the radar parameters can be found on the radar web site `http://www-das.uwyo.edu/wcr`. The WCR/UWKA installation takes advantage of four fixed antennas. Two point side and side-forward and two point down and down-forward from the aircraft. For this study, primarily the *Horizontal Beam Dual-Doppler* (or HBDD) mode was employed (see Fig. 1), synthesizing velocity fields across horizontal planes and analogous to the *Vertical Plane Dual-Doppler* (or VPDD) utilized in DVH05. Additional support to the analysis came from data collected in 'profiling' modes, namely single-Doppler *up-down* and *side-down* profiling modes. They respectively allowed to scan a vertical plane above and below the aircraft, or a starboard horizontal plane and a vertical plane below the aircraft. The closest usable radar rangegates were at ∼100 m from the aircraft. For more details about the radar installation, the available scanning modes, calibration, dual-Doppler retrieval procedure and data uncertainty analysis refer to Damiani and Haimov (2005a,b), DVH05.

Measured reflectivity has an estimated absolute accuracy of ±2.5 dB, and a precision, for the full dynamic range of the receivers, better than 1 dB. The sensitiv-

*Corresponding author address: Rick Damiani, Dept. of Atmos. Sci., University of Wyoming, 1000 E. University Ave., Laramie WY, 82071; E-mail: rickdami@uwyo.edu

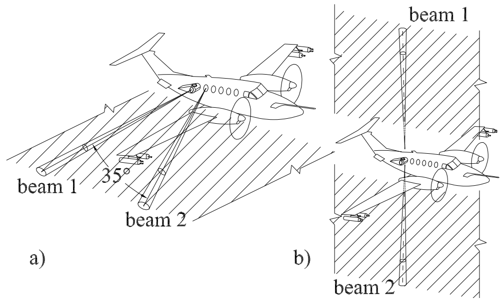

FIG. 1. Two WCR dual-beam antenna configurations aboard the UWKA relevant for this study: a) HBDD; b) up-down profiling.

ity (minimum detectable signal) of the radar varies with the antenna used, with the side-forward and side antenna channels being the least and the most sensitive ones. The minimum detectable signal for 250 ns (500 ns) pulses and the commonly used 84 averaged pulse pairs for velocity measurement (168 averaged pulses for reflectivity) varied from -28 to -21 dBZ (-34 to -26 dBZ) at 1 km. The sensitivity of the slanted-pointing antennas is the limiting factor for the dual-Doppler retrieval. No correction for attenuation was applied to the reflectivity due to the unknown and highly non-homogeneous distribution of liquid water in cumulus clouds. In the vertical planes, the terminal velocity of the scatterers was not removed. This particle fall-speed effect is discussed in detail in DVH05. Attenuation and insufficient sensitivity are responsible for some lack of data in weak-reflectivity areas of the clouds.

The reflectivity data in this study were thresholded based on 2.5-3 standard deviations of the noise. The accuracy of the calculated velocities is on the order of 1-2 m s^{-1}. The plots shown in the following sections present vector fields overlaid on the reflectivity fields (filled contours of reflectivity factors, mm^{6}m^{-3}in dBZ). Selected streamlines were plotted with solid lines after integration of the 2-D fields. Mean horizontal winds, measured at flight level, were subtracted from the data, therefore the kinematics can be interpreted as relative to the mean wind translating frame.

3. HICU03 CLOUD AND ENVIRONMENT CHARACTERISTICS

The target of this investigation were moderately deep continental cumuli developing over the southeastern part of the state of Wyoming in July-August, 2003. Clouds had high bases, near 5 km MSL and at ∼-5 °C on most days, and grew in a dry environment. On most days, the clouds were not constrained by significant inversions, while cloud bases were in proximity of a wind shift zone at the border of a relatively dry layer. The lapse rate was approximately dry adiabatic below 600 hPa, and close to moist adiabatic above 500 hPa. The available soundings are not very accurate since the data were collected in regions and time intervals different from those of the actual investigation. Therefore, details such as cloud base altitudes and atmospheric stability parameters could not be computed precisely. Visual estimates and reverse adiabatic liquid water calculations were used to retrieve cloud base heights. The WCR did not detect cloud bases due to insufficient sensitivity in most of the cases.

During their growing phases, the clouds were characterized by very sharp edges, and exhibited an ebullient appearance. Our observations were limited to isolated cumuli and, in certain instances, to towers or emerging turrets within larger clusters. Cloud depth extended up to 3 km. Maximum cloud diameters were ∼3.5 km with unitary aspect ratios. Recorded vertical in-cloud velocities ranged from -10 to 10 m s^{-1}, and radar echoes ranged between -30 and 10 dBZ. More information on the basic properties of the clouds studied can be found in DVH05.

In DVH05, the authors report evidence for the pulsating nature of the clouds sampled, classifying them as *multi-thermal* systems, emphasizing the bubble character of the updrafts. The observed thermals enclose well-defined vortical structures, resembling the classical model of a buoyant vortex-ring (Turner 1973), with strong divergence at the top and convergence at the bottom. The buoyant toroid rises at about half the maximum updraft speed found along the vertical axis. Episodes of ambient air entrainment and hydrometeor recycling are associated with this main circulation. In addition, the vortical motion displaces and sheds hydrometeors encountered at the leading edge of cloud-intruding thermals. Ambient winds and shear within the cloud layer depth play a key role in affecting the cloud development. When the shear exceeds roughly 0.003 s^{-1}, the emerging turrets are tilted, with predominant updrafts on the upshear region and downdrafts on the downshear one. The tilt effectively couples the vertical and the horizontal fields of motion. A slanted rise of the updrafts was also observed with embedded asymmetrical vortex-rings. In more moderate shear cases, the updrafts were upright with almost symmetrical downdrafts at their edges.

In Fig. 2, radar reflectivity and Doppler velocity fields in a vertical plane above and below flight level are shown together with in situ (flight-level) measurements of liquid and ice water contents (LWC, IWC), and air gust vectors, for a typical cloud investigated during the HiCu03 field campaign. The transect reveals the ascent of a new thermal into an already mature congestus. The cloud top rose at an approximate rate of 2.5 m s^{-1}. This rate of rise, at about one half the maximum vertical speed within the updraft core. Reflectivity is higher at the top and sides of the updraft. The updraft is filled with cloud droplets (mean diameter 10-20 µm) and a few small ice particles. The air temperature measured at cloud-top was ∼-21 °C. The largest hydrometeors, namely ice up to 1 mm in diameter recorded by the in situ probes, were present mostly in the descending regions and gave rise to the strongest radar echoes. The lack of radar data in the middle of the cloud is due to the radar returned power falling below the noise threshold. Cloud base, estimated from thermodynamics and visual observations, was around 5900 m MSL. The downdrafts are located at the edges of the updraft and at the cloud boundaries. Strongly diverging gust vectors

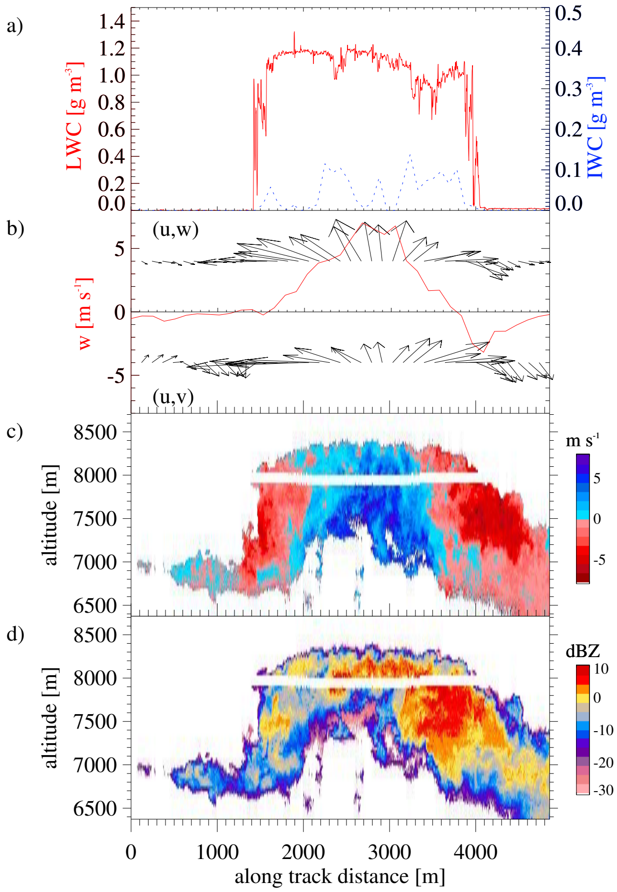

FIG. 2. Up-down profiling pass at a Cu con, conducted on 16 July, 2003 at 20:27UTC. a) LWC and IWC in g m^{-3}; b) gust probe measured air vertical velocity w in (m s^{-1}), with overlaid 1-s gust vectors in the vertical (u,w) and horizontal plane (u,v) (deviations from a mean horizontal wind); c) Doppler velocity and reflectivity contours in the vertical plane above and below the AC. Flight level is in the middle of the radar 'blind zone' (blank stripes in panels c) and d)) at 7900 m MSL. Aircraft heading is $\sim$22°.

(derived from flight level measurements) are visible at the top of the updraft. In the horizontal plane (u,v), gust vectors show that the flow abruptly changes direction going from the edges of the cloud toward its interior, and this corresponds well with the transition between updraft and descending flow. This directional change was recorded in many cloud penetrations during this study and will be discussed in more detail below. Note, also, that the downdrafts extend to the clear-air volumes outside the cloud boundaries.

4. THE NATURE OF AIR MOTIONS IN HORIZONTAL CLOUD TRANSECTS

4.1 *Evidence of Gradients and Structures Comparable to Those in the Vertical*

HBDD analyses revealed that horizontal cross-sections of the clouds exhibit velocity gradients and length scales comparable to those in the vertical. An example is shown in Fig. 3, where a congestus is horizontally scanned at approximately 6100 m MSL, at about 1 km below cloud top. Filled contours of radar reflectivity factors are shown in the background with retrieved 2-D velocity vectors.

The reflectivity field confirms the high variability of the hydrometeor density within congestus. The main reason is that at this stage the cloud already had a sequence of thermals rise past the observation level, as seem from previous vertical sections (not shown for sake of brevity). Toward the top of the image, the lack of data is again attributable to the low returned power from the updraft cores filled with small droplets, and partially to attenuation effects. The superimposed track (thick solid line) in Fig. 3 corresponds to a previous pass traversing the volumes of the main updrafts.

A counterclockwise-rotating vortex is centered at[1] x =4100 m, y =2300 m; the size of the vortex is about 500 m. Two regions of flow horizontal divergence are visible at [x,y]=[4800,1700] m and [x,y]=[6200,1300] m respectively (labeled '1' and '2' in Fig. 3). The maximum calculated horizontal divergence in the latter region (over a circle of diameter $\sim$500 m) was 0.09 s^{-1}. The divergent pattern on the left-hand (western) side of the image is characterized by stronger reflectivity than the one on the right-hand (eastern) side. Since areas of divergence are associated with the tops of thermals (cf. DVH05), the two regions in Fig. 3 may well correspond to two separate updrafts, and the image portrays two thermals at two different stages. The updraft on the west (left-hand) side is mainly below flight level, and its cap, filled with suspended older hydrometeors and ice, presents the largest reflectivity; the other updraft may have exceeded flight altitude, so that the horizontal scan captures its weak-echo core. This is analogous to what was observed in vertical transects during the rise of the thermal within the cumulus depicted in Fig. 2. The distance between the two divergent flow regions is about 1600 m, comparable to the distance between the updrafts encountered in previous penetrations.

Fig. 4 shows an HBDD pass for the same cloud as in Fig. 2. In this case, a couplet of low vs high reflectivity is seen aligned with the ambient shear direction. The weak-echo region to the south-west is associated with flow radially diverging from a center location at [x,y]=[3000,1600] m (marked with a circle in the figure). The ambient wind at flight level was 260° at 11.8 m s^{-1}, and the vertical shear within the cloud layer was $\sim$0.006 s^{-1} and directed north-east. The flow directed against the shear direction in the western sector of the cloud is confirmed by the in situ data of Fig. 2. The magnitude of the horizontal winds in both the up/down and the HBDD passes is about 3 m s^{-1} (in the mean-wind relative frame), and the direction is consistently due south-west, thus the cloud volumes associated with the updraft top were characterized by lesser horizontal momentum than the mean

[1] x,y denote the abscissa and ordinate values of the plots.

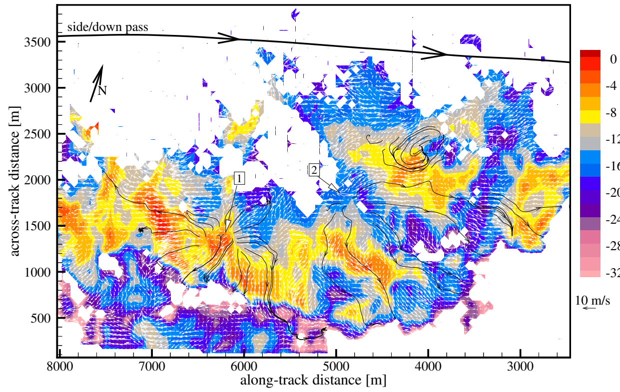

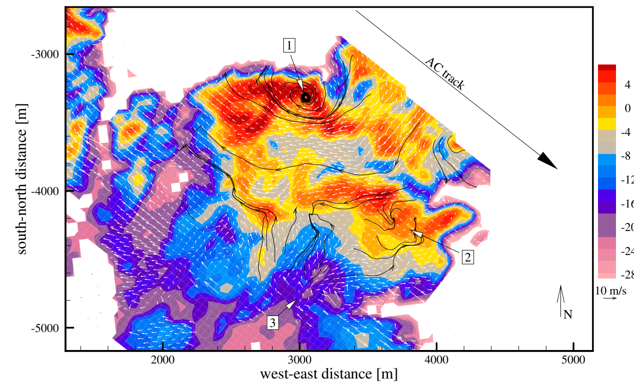

FIG. 3. HBDD analysis of a Cu con, conducted on 26 August, 2003 at 17:29UTC. Reflectivity (from the side-pointing beam) filled contours (dBZ) with superimposed dual-Doppler retrieved horizontal velocity field. AC heading is 252°; grid resolution is approximately 44×47 m^2. Thin solid lines are streamlines. The thick solid line represents the AC trajectory of a previous pass. The arrow labeled with 'N' indicates true north. Two regions of horizontal divergence are denoted by label '1' and '2'.

FIG. 5. As in Fig. 3 for an HBDD analysis of a Cu con, conducted on 17 July, 2003, at 20:50UTC. AC heading is 125°; grid resolution is approximately 45×45 m^2. Labels '1', '2' and '3' denote two vortical structures and a horizontal divergent flow region.

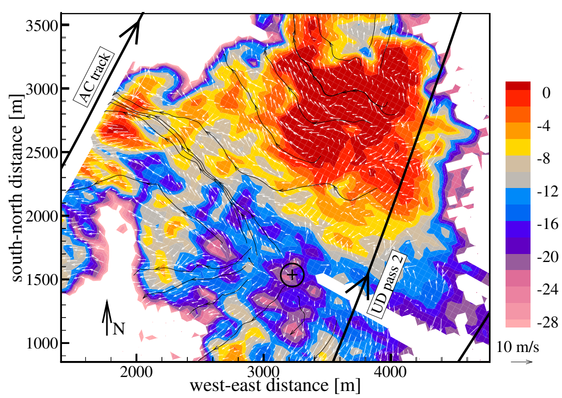

FIG. 4. As in Fig. 3, for an HBDD analysis of the top region of the congestus in Fig. 2, conducted on 16 July, 2003 at 20:31UTC. Grid resolution is approximately 45×47 m^2. Thick solid lines are the AC air-relative tracks of the pass in Fig. 2 (denoted by the label 'UD pass 2') and of the current. The mark in the lower portion of the image identifies the location of horizontally diverging flow.

wind at that level. Inaccuracy in the estimated shear cannot account for a 180° reverse tilt of the updraft. Interaction with descending air parcels or with other thermals might have caused the updraft to be predominantly directed toward the south-west. The higher reflectivity sector, to the north-east, shows chaotic flow. The maximum reflectivity in Fig. 4 is 5 dBZ, an increase of about 10 dBZ over the previous 8 min mostly due to glaciation occurring at cloud top at temperatures near -20 °C.

4.2 *Vertical Vorticity Structures and Ambient Air Intrusions*

Vortical structures were frequently observed in the horizontal cross-sections. The vortices had characteristic diameters of about 500 m, and persisted for several minutes. An example is shown in Fig. 3, and a further one is given in Fig. 5. For the case in Fig. 5, the mean wind at scan level in proximity of the cloud was measured to be 242° at ∼7 m s^{-1}, and the shear was 0.005-0.006 s^{-1} roughly directed north-east. The transect was executed at an altitude of about 7900 m MSL, near the top of a turret emerging from a cumulus congestus.

The reflectivity is stronger in the northern (upper in the figure) part of the cloud, with values reaching 6-8 dBZ. In the southern portion of the cloud the values are between -10 and -20 dBZ. The striking feature visible from the velocity field is the well defined clockwise-rotating vortex centered at x =3100 m and y =-3400 m (label '1' in the figure). The strongest reflectivity is just to the left of the vortex center. Adjacent to the circulation, in the central part of the cloud, the echoes are slightly weaker (-6 dBZ), and the vectors show an intense air flow from the east. This region has the characteristics of the updraft core. Once again the flow close to cloud top (in the usual wind-relative frame of reference) is directed against the ambient vertical wind-shear. Further to the east-south-east (right in the figure, label '2'), the reflectivity is relatively large and the velocity field suggests a counterclockwise circulation. The mean vertical vorticity, calculated over regions of 500 m in diameter, is ∼0.04 s^{-1} in both the clock and counterclockwise circulations. Maximum vorticity on a 100 m scale in the northern circulation is about 0.08 s^{-1}. The region to the south (the upshear region) exhibits radially diverging flow from a center location at [x,y]=[2500,-5000] m (label '3' in Fig. 5). To the north-east of the two vortices, at [x,y]=[3200,-3200] m and [x,y]=[3800,-4000] m, there is evidence of dry air intrusion, confirmed by the velocity field and weak echoes extending toward the interior of the cloud. This is typically encountered when the eddies are located in proximity of the cloud boundaries.

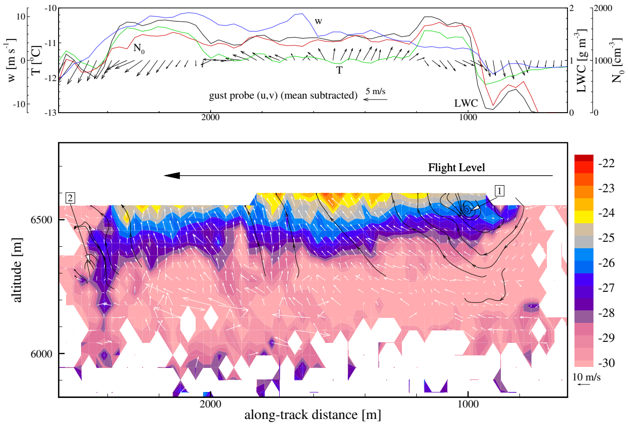

FIG. 6. VPDD analysis of a Cu con, conducted on 20 July at 19:03UTC. Reflectivity (from the straight beam echoes) field with superimposed dual-Doppler retrieved horizontal velocity field. AC heading is 245°; grid resolution is approximately 30×47 m^2.Upper panel reports in situ data: w (m s^{-1}) air vertical velocity, LWC (g m^{-3}), T (°C), and vertical plane gust vectors (relative to the mean wind at flight level,i.e., 314° at 6 m s^{-1}). Labels '1' and '2' denote circulations.

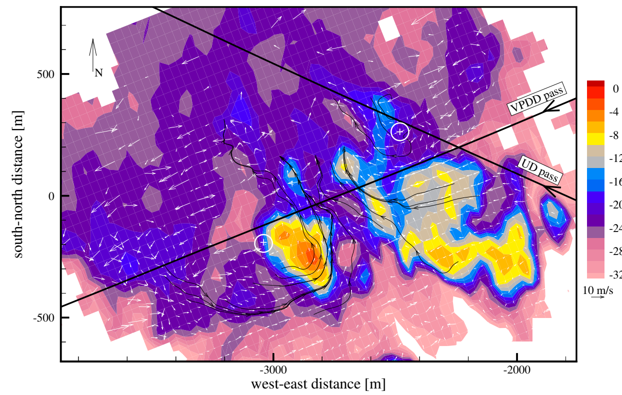

FIG. 7. As in Fig. 5 for an HBDD analysis at the cumulus in Fig. 6. Time 19:06:30UTC. AC heading is 245°. The air-tracks from other passes are also shown with solid lines, and the label 'VPDD pass' denote the pass whose results are illustrated in Fig. 6. Grid resolution is approximately 32×45 m^2. The circles mark the circulations' centers.

4.3 *A Mechanism for Vertical Vorticity Generation*

In the following, cases are discussed for which both horizontal and vertical plane measurements were executed within short time intervals, in order to shed some light on possible sources of the observed vertical vorticity.

Fig. 6 shows measurements from a towering congestus performed on 20 July, 2003 between 19:03 and 19:17 UTC. Winds were north-westerly with a shear of 0.003 s^{-1} directed east. The first penetration was at 6700 m MSL, as cloud-top was reaching about 300 m above the flight level. Cloud base was at about 5000 m MSL. No ice was detected during the penetration, and the radar echoes are weak. The lack of data ∼700 m below flight level is a consequence of attenuation and signal return that did not exceed the noise threshold. The LWC trace shows two major peaks and two downward spikes, just before the cloud outer boundaries. The gust-probe derived air-velocity vectors indicate divergence and a fairly uniform updraft within the tower, with a peak at 10 m s^{-1} and with weak descending flow at the edges, outside the cloud. This pattern in the vertical velocity is mirrored by the radar retrieved motions. In particular, a distinct clockwise circulation is visible centered at [x,y]=[1000,6500] m (label '1' in Fig. 6) and, with it, a trace of possible dry air intrusion from the side. To the west (left in the figure, label '2'), there is an indication of counterclockwise overturning of the flow. The following pass was performed about three minutes later in HBDD mode, and the results are given in Fig. 7. The radar echo was weak and the retrieved velocity field is consequently noisy. However, some patterns are recognizable both in the reflectivity and velocity fields. The velocity vectors wrap around two major circulation centers located at [x,y]=[-3000,-200] m and [-2500,200] m (marked with small circles in the figure). The higher reflectivity values are found along the perimeters of the circulations and are separated in the middle of the cloud where the flow streamlines converge between the two circulations. This is consistent with the LWC trace in Fig. 6. The gust-probe horizontal wind vectors in Fig. 6 support the vortical patterns found in Fig. 7, and place them at the edges of the updraft. Within the updraft, the diverging flow is mainly directed northward. The westerly shear cannot be responsible for a northward tilt of the updraft. The divergence at the top of the updraft could in part justify the northward directed flow (in a reference frame relative to the mean wind, i.e., 314° at 6 m s^{-1}). However, this flow pattern could be explained if a buoyant vortex-ring were tilted against the mean wind direction.

A further example of strong vorticity generated in the horizontal plane is given by data from an isolated congestus in Figs. 8-9. This time the flight level was at about 8200 m MSL; the winds were stronger (i.e., 294° at 13 m s^{-1}) and the cloud top was about 100-200 m above flight altitude. The first penetration (executed in VPDD mode, cf. Fig. 8) recorded no measurable ice concentration whereas about 6 min later, with no sign left of ascending air, the maximum LWC decreased by about 50%, the IWC peaked at ∼0.2 g m^{-3}, and the reflectivity maxima increased from -15 to 0 dBZ. Well-defined circulations are visible at the edges of the updraft in Fig. 8 (labels '1' and '2' point to the centers of the vortices). The reflectivity associated with the rising quadrants of the vortex on the right-hand (eastern) side of the image (note the tongue of ∼-21 dBZ at [x,y]=[2900,7800] m) is suggestive of a mixing process with ambient dry air entrapped by the circulation. Assuming that the vertical transect was in proximity of the updraft center, the image also shows that the updraft was slightly tilted toward the north-north-west, or upwind (the ambient winds at flight level were north-westerly). The HBDD pass shown in Fig. 9 was performed about 200 m higher than the first VPDD

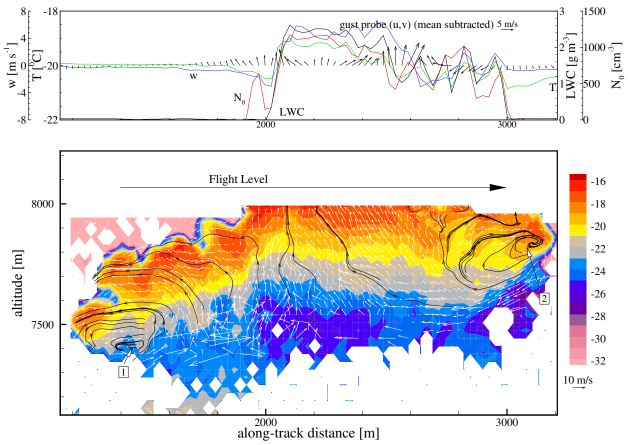

FIG. 8. VPDD analysis of a Cu con, conducted on 20 July, 2003, at 19:57UTC. Reflectivity (from the straight beam echoes) field with superimposed dual-Doppler retrieved horizontal velocity field. AC heading is 148°; grid resolution is approximately 25×35 m^2. Upper panel reports in situ data: w (m s^{-1}) air vertical velocity, LWC (g m^{-3}), T (°C), N_0 total number concentration from FSSP-100, and horizontal plane gust vectors (relative to the mean wind at flight level, i.e., 294° at 13 m s^{-1}). Labels '1' and '2' point to the centers of two vortices.

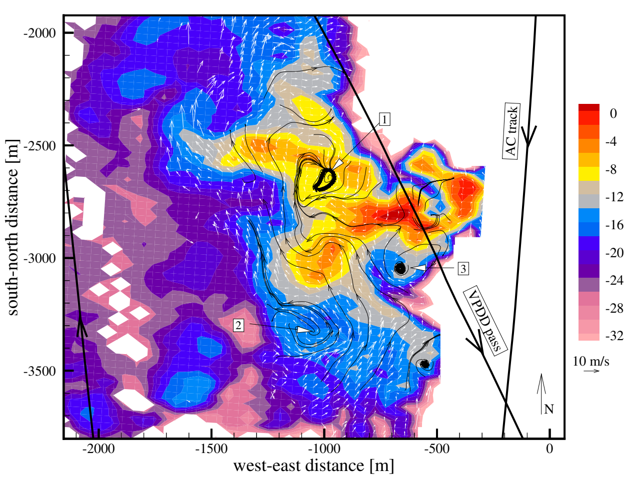

FIG. 9. As in Fig. 7 for an HBDD analysis at the cumulus in Fig. 8. Time 20:01:30UTC. AC heading is 180°. Thick solid lines indicate the air-tracks from the current and other passes; that labeled with 'VPDD pass' refers to the pass in Fig. 8. Grid resolution is approximately 31×46 m^2. Mean wind 318° at 11.9 m s^{-1}. Labels '1', '2' and '3' refer to circulations.

penetration. The cross-section captures a well defined clockwise circulation centered at [x,y]=[-1100,-2600] m (label '1' in Fig. 9). From the reflectivity field, the hydrometeors appear concentrated mainly along the perimeter of the circulation. At [x,y]=[-1100,-3400] m (label '2') a counterclockwise-rotating vortex is in a region of weaker radar echoes. Another vortex, with evidence of dry air intrusion, can be seen at [x,y]=[-600,-3050] m (label '3'). Further ambient air entrainment is visible at [x,y]=[-700,-2600] m, in part favored by the large circulation to the north.

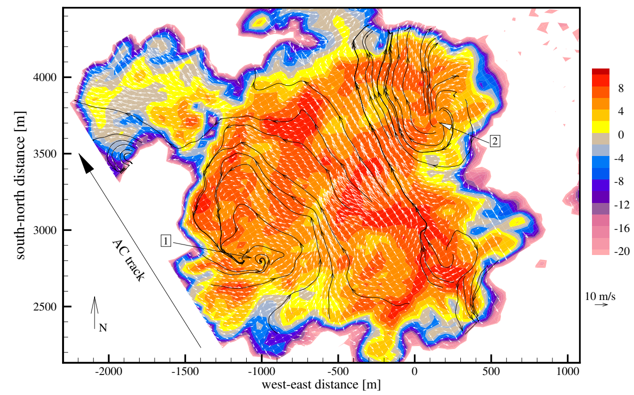

FIG. 10. As in Fig. 7 for an HBDD analysis at an isolated congestus. The scan was performed on 12 July, 2003; Time 19:35:30UTC. AC heading is 330°. Grid resolution is approximately 35×46 m^2. Mean wind at the scan altitude of 7800 m MSL is 307° at 17 m s^{-1}. Labels '1' and '2' point to the centers of the vortices.

The maximum vorticity (not shown) is found in the southernmost vortex (∼0.15 s^{-1}), whereas the minimum (∼-0.1 s^{-1}) in the vortex to the east (label '3' in Fig. 9). For comparison, the vorticity magnitude calculated within the vertical transect of Fig. 8, exceeds 0.12 s^{-1}. The two vortices (centers at [x,y]=[-1100,-3400] m and [x,y]=[-600,-3050] m, labels '2' and '3' in Fig. 9) represent a counter-rotating vortex pair (CVP). CVP's can be the result of tilted vortex rings in the ascending thermals. The sense of rotation of the two vortices is consistent with the tilt of the thermal toward the north-west, against the mean wind (cross-flow) direction. Besides the cross-flow effect, local shear in the winds and interaction among thermals can also be responsible for the tilting of the toroids. The shear in the 200 m altitude difference between the two scans in Figs. 8-9, for example, is actually directed west and measured 0.005 s^{-1}.

Another striking CVP arrangement (labels '1' and '2') is evident in Fig. 10 showing an HBDD synthesis for a cloud investigated on 12 July, 2003. The two vortices occupy the majority of the cloud region. The strong southeasterly flow between the vortices indicates that volumes in the middle of the cloud have lesser horizontal momentum than the mean north-westerly winds at that altitude. That region in the middle is likely to be the location of the updraft core. On this day, the shear in the cloud layer was calculated to be negligible, except for about 0.01 s^{-1} in the upper ∼500 m of the cloud layer. Maximum vorticity is 0.15 and 0.1 s^{-1}, for the western and eastern vortex respectively.

Further support to a connection between the circulations observed in the vertical and horizontal planes is provided by the up/down profiling pass in Fig. 11, taken from (DVH05). The figure shows that the double meridional circulation of the rising vortex ring in the vertical plane (panel b, (u,w)) is accompanied by evidence of a CVP in

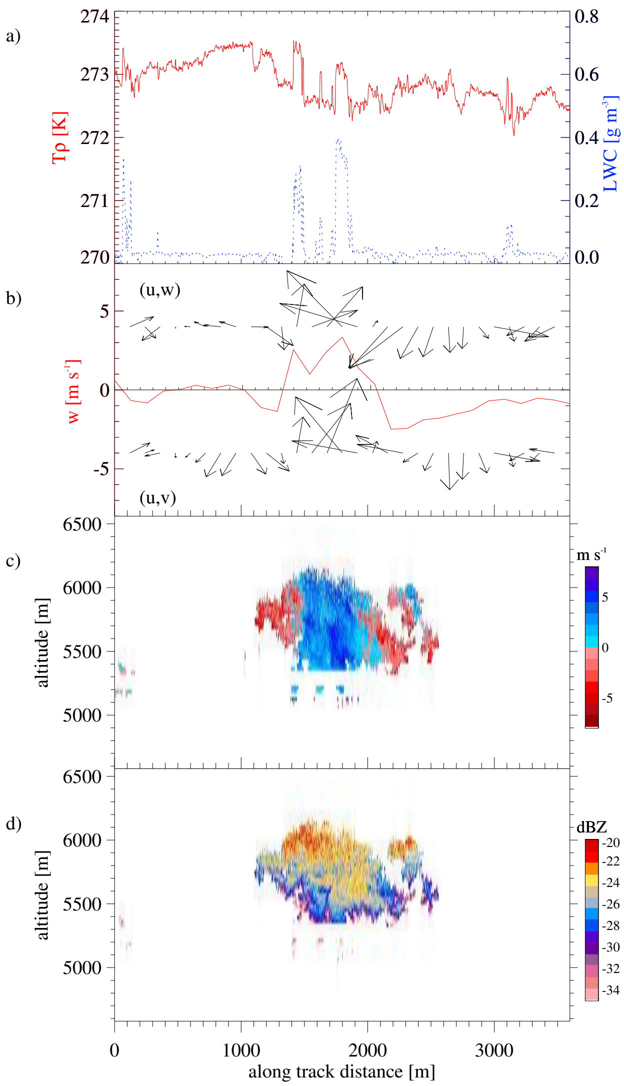

FIG. 11. Results of an up/down profiling scan of an isolated growing cumulus carried out on 19 July, 2003; time 19:45 UTC. Approximate aircraft track heading was 350°. Mean wind at flight level: 300° at 4.5 m s^{-1}. The upper panels show in situ variables collected at flight level (5250 m MSL): a) density temperature (T_ρ, K) and liquid water content (LWC from DMT probe, g m^{-3}); b) gust probe vertical velocity (w, m s^{-1}), and vertical and horizontal plane vectors calculated along the aircraft track every ∼1 s (mean horizontal wind removed). The bottom panels show the WCR Doppler-retrieved vertical velocity (c) and reflectivity (d).

the horizontal plane (panel b, (u,v)). The transition from updraft to downdrafts is in fact characterized by a 180° rotation of the horizontal wind vectors. The vectors are oriented toward the west in the updraft region.

5. DISCUSSION

The analyses of horizontal air motions in growing turrets showed that the flow structures are highly complex. Regions of strong divergence, mostly associated with weak radar reflectivity, are believed to be the tops of updrafts for two main reasons. Firstly, updrafts are characterized by lower radar echoes than downdrafts. Secondly, the thermals embed a vortex-ring type of circulation with strong divergence at the top. In more mature clouds, new updraft pulses tend to suspend, at their leading edges, ice crystals or small drops already present within the cloud volumes. Consequently a narrow band of strong reflectivity at its leading edge can accompany the intrusion of a new thermal.

The rate of rise of the vortex-ring enclosed within a thermal can be roughly estimated by an analysis of the mass fluxes across the surfaces of a control volume in the form of an upright cylinder centered in a resolved horizontal divergence region. The ratio of the horizontal mass flux across the lateral surface of the cylinder to the vertical flux across its lower base was in the range ∼0.4-0.6. These values indicate that the thermals rose at about 40-60% of the updraft core velocities, in agreement with other observations which find the rate of rise of buoyant vortex rings to be about one half the maximum updraft velocity (e.g., Woodward (1959); Turner (1962); Telford (1988); Zhao and Austin (2005),DVH05).

Horizontal air flow in developing clouds often showed organized vortical structures lasting in some cases over 5 min.

The location of the vortices, at the periphery of the ascending updraft cores, proves that they were not part of strong, vertically aligned, helical flows, and we have no evidence for rotating updrafts.

Tilting of horizontal vorticity near the surface due to ambient vertical shear, important in the generation of dust-devils and in super-cell thunderstorm dynamics (e.g., Maxworthy 1973; Davies-Jones 1984; Klemp 1987), cannot explain the existence of the observed vortices either.

Rotating vertical columns and CVP's have been observed along the flanks and downstream of buoyant plumes and non-buoyant jets (e.g., Church et al. 1980; Kelso et al. 1996; Lim et al. 2001; Cunningham et al. 2005). The generation of columnar dust-devil-type vortices in the wakes of plumes is still unclear, but an interaction of ambient vorticity (associated with wind vertical shear) and plume baroclinically generated vorticity is considered to be key to their existence. These vortices have been observed to shed in an oscillatory fashion from the main updraft volumes and advect downstream with the cross-flow, resembling the classic vortex-shedding behind bluff-bodies. Vertical vorticity in CVP's is also found within rising plume (or jet) volumes, and can lead to a bifurcation of the plumes. This vorticity gets eventually tilted in the streamwise direction, forming horizontally aligned CVP's. For the cases studied here, the lack of continuity in the updraft columns from their sources, and the observation of strong vertical vorticity (i.e., suggesting it cannot be yet tilted back in the horizontal direction, even though the level of observation is considerably distant from the thermal release altitude) automatically rule out these mechanisms for vertical vorticity generation.

Another source of vertical vorticity is the horizontal (azimuthal) vorticity contained in the vortex-rings within the rising thermals. The cross-flow action by the horizontal winds can tilt the rings and thus generate vertically oriented CVP's. There are two possibilities for a vortex ring to be tilted. If the updraft rises in a slanted fashion from the surface, the toroidal circulation axis will be aligned with the slanted path of the updraft. A new updraft pulse, triggered by latent heat release, can cause horizontal vorticity to be concentrated in the shear layer at its edges due to transverse density gradients (enhanced by different levels of mixing from the core towards the edges). In contrast, if an upright vortex ring encounters unidirectional shear, the toroid axis will tilt *against* the cross-flow direction (e.g., Chang and Vakili 1995; Diez et al. 2003), due to the torque exerted by Kutta-Joukowski lift forces (Magnus effect) that develop in opposite directions along the upshear and downshear ring arcs. This action within the thermal opposes the normal downshear bend of the ascending air column, and plays a dynamic stabilization role similar to a gyroscopic effect. In cases where the mean ambient vertical shear was significant (say >0.003 s^{-1}), a preferential organization of updrafts and downdrafts was evident. The updrafts tended to appear within the upshear sector of the cloud, decaying, giving way to downdrafts and collapsing turrets, on the downshear side of the cloud. This spatial arrangement was observed since the initial studies of Malkus (1954); Ackerman (1958); Scorer (1958) as well as in many recent studies (e.g., Rogers et al. 1985; Perry and Hobbs 1996; Vaillancourt et al. 1997). We found many examples of reflectivity patterns (confirmed by visual appearance) indicating upright vortex-ring axes, rather than aligned with the slanted updraft trajectory.

Our analyses, show that ascending cloud-volumes are generally characterized by lesser horizontal momentum than the surroundings, and aligned in path tilted in the direction opposite to the mean ambient wind, or to the mean vertical shear vector (which frequently was along the wind direction at high altitudes). Simple calculations of the drag exerted on rising thermals by the ambient winds, under the conditions of wind shear encountered, indicate that the thermals should possess the same horizontal momentum than the ambient fluid volumes moving with the mean wind speeds. However, the vertical stabilization effect discussed above can lead to reduced horizontal momentum of the thermal cores. Experiments (e.g., Diez et al. 2003) and numerical simulations (e.g., Chang and Vakili 1995) illustrate that rising vortex-rings in cross-flow tend to oppose or even overcome the mean-wind advection.

Fig. 12 illustrates an ideal toroidal thermal tilted by the action of the cross-flow. This configuration not only would yield lesser horizontal momentum observed in the cross-sections, but it also explains the presence of vorticity located at the periphery of the ascending thermal cores. The vertical vorticity can be seen concentrated in CVP's, or at least in two distinct and opposite blobs at various levels, in accordance with the foregoing results.

Interactions with other ascending bubbles could also

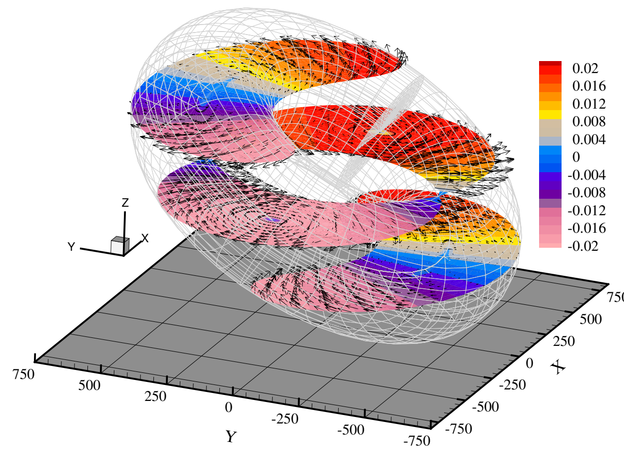

FIG. 12. Ideal model of tilted toroidal thermal with filled contours of vertical vorticity (s^{-1}) at various horizontal cross-sections. The meridional velocity is linearly distributed with the tube radius with maximum velocity equal to 5 m s^{-1} and the average azimuthal vorticity is 0.04 s^{-1}. The toroid axis is tilted by 30°.

cause the tilting of the vortex rings and the generation of more complex patterns in the vertical vorticity. This process is supported by the simulations of Shapiro and Kogan (1994), where a multi-cell convective cloud system is seen to generate vertical vorticity by tilting of horizontal vorticity associated with the vortex-rings of the individual cells, due to the interference and mutually induced velocities of the single convective entities. The size ($\sim$500 m) and the intensity ($\sim$0.04-0.1 s^{-1}) of the eddies found in horizontal planes are comparable to their counterparts in vertical planes, consistent with the hypothesis of toroid tilting.

6. SUMMARY

The model of multi-thermal cumulus presented in DVH05 is refined and extended in the present study by accounting for the tilting and slanted rise of the toroidal thermals.

Regions of horizontal flow divergence were collocated with weaker radar echoes than the surroundings. This divergence is thought to mark the tops of rising toroids.

When the ambient vertical shear in the cloud layer exceeded roughly 0.003 s^{-1}, the updrafts were found on the upshear sector of the cloud with downdrafts on the downshear one.

Vertically oriented vortices were often encountered. The intensity (mean 0.04 s^{-1}, peaks greater than 0.1 s^{-1}) and size ($\sim$500 m in diameter) of the vortices are comparable to those found in vertical transects. Out of thirty-three cases investigated in HBDD mode, nineteen presented a clear indication of vertical vorticity, although in some cases the vortices were either individual structures or more randomly appearing eddies. Radar retrieved velocity fields or in situ gust vectors indicated CVP's for twenty-three clouds; fifteen cases with strong evidence.

The main mechanism for the formation of CVP's was identified in the tilting of azimuthal vorticity of the rising vortex-rings. The sense of rotation of the vortices and their spatial location suggest a tilt of the toroid against the mean wind direction.

The location of the vortices at the periphery of the updrafts, and hence in proximity of the downdrafts, can favor the recycling of precipitating hydrometeors. Entrainment and ambient air intrusions were found associated with the inflow quadrants of the vortices near the edges of the clouds. The gradients of Reflectivity gradients at cloud edges were high (up to 0.2-0.4 dBZ m^{-1}) where the air velocity was mostly tangent to the boundary, and half as large where the velocity was mostly normal to the edges ($\sim$0.1-0.2 dBZ m^{-1}).

The horizontal fields of motion reveal gradients and velocities (in frames relative to the ambient mean winds) comparable to those measured in the vertical. These motions appear to be further manifestations of a coupling between vertical and horizontal motions.

Acknowledgments. The author would like to thank the colleagues in the Department of Atmospheric Science at the University of Wyoming and the UWKA facility team involved in the HiCu03 experiment. This study was supported by NSF Grant ATM-0094956.

7. REFERENCES

Ackerman, B., 1958: Turbulence around tropical cumuli. *J. Meteor.*, **15**, 69–74.

Blyth, A. M., 1993: Entrainment in cumulus clouds. *J. Appl. Meteor.*, **32**, 626–641.

Blyth, A. M., W. A. Cooper, and J. B. Jensen, 1988: A study of the source of entrained air in Montana cumuli. *J. Atmos. Sci.*, **45**, 3944–3964.

Carpenter, R. L. J., K. K. Droegemeier, and A. M. Blyth, 1998: Entrainment and detrainment in numerically simulated cumulus congestus clouds. Part III: Parcel analysis. *J. Atmos. Sci.*, **55**, 3440–3455.

Chang, Y. K. and A. D. Vakili, 1995: Dynamics of vortex rings in crossflow. *Phys. Fluids*, **7**, 1583–1597.

Church, C. R., J. T. Snow, and J. Dessens, 1980: Intense atmospheric vortices associated with a 1000 MW fire. *Bull. Amer. Meteor. Soc.*, **61**, 682–694.

Cunningham, P., G. S. L., M. Y. Hussaini, and R. R. Linn, 2005: Coherent vortical structures in numerical simulations of buoyant plumes from wildland fires. *Int. J. Wildland Fire*, **14**, 61–75.

Damiani, R. and S. Haimov, 2005a: High resolution airborne radar dual-Doppler-part I: Technique. *IEEE Trans. Geosci. Remote Sensing*, submitted.

— 2005b: High resolution airborne radar dual-Doppler-part II: Error sources. *IEEE Trans. Geosci. Remote Sensing*, submitted.

Damiani, R., G. Vali, and S. Haimov, 2005: The structure of thermals in cumulus from airborne dual-Doppler radar observations. *J. Atmos. Sci.*, submitted.

Davies-Jones, R., 1984: Streamwise vorticity: The origin of updraft rotation in supercell storms. *J. Atmos. Sci.*, **41**, 2991–3006.

Diez, F. J., L. P. Bernal, and G. M. Faeth, 2003: Round turbulent thermals, puffs, starting plumes and starting jets in uniform crossflow. *ASME J. Heat Transfer*, **125**.

Johari, H., 1992: Mixing in thermals with and without buoyancy reversal. *J. Atmos. Sci.*, **49**, 1412–1426.

Kelso, R. M., T. T. Lim, and A. E. Perry, 1996: An experimental study of round jets in cross-flow. *J. Fluid Mech.*, **306**, 111–144.

Klemp, J. B., 1987: Dynamics of tornadic thunderstorms. *Ann. Rev. Fluid Mech.*, **19**, 369–402.

Lim, T. T., T. H. New, and S. C. Luo, 2001: On the development of large-scale structures of a jet normal to a cross flow. *Phys. Fluids*, **13**, 770–775.

Malkus, J. S., 1954: Some results of a trade-cumulus cloud investigation. *J. Atmos. Sci.*, **11**, 220–237.

Maxworthy, T., 1973: A vorticity source for large-scale dust devils and other comments on naturally occurring columnar vortices. *J. Atmos. Sci.*, **30**, 1717–1722.

Morton, B. R.: 1997, *The Physics and Parameterization of Moist Atmospheric Convection*, Kluwer Academic, The Netherlands, volume Vol 505, chapter Discrete dry convective entities I: Review. 143–173.

Pazmany, A., R. E. McIntosh, G. Vali, and R. D. Kelly, 1994: An airborne 95 GHz dual-polarized radar for cloud studies. *IEEE Trans. Geosci. Remote Sensing*, **32**, 731–739.

Perry, K. D. and P. V. Hobbs, 1996: Influences of isolated cumulus clouds on the humidity of their surroundings. *J. Atmos. Sci.*, **53**, 159–174.

Rogers, D. P., J. W. Telford, and S. K. Chai, 1985: Entrainment and the temporal evolution of the microphysics of convective clouds. *J. Atmos. Sci.*, **42**, 1846–1858.

Sanchez, O., D. Raymond, L. Libersky, and A. Petschek, 1989: The development of thermals from rest. *J. Atmos. Sci.*, **43**, 2708–2718.

Scorer, R. S., 1957: Experiments on convection of isolated masses of buoyant fluid. *J. Fluid Mech.*, **2**, 583–594.

— 1958: *Natural Aerodynamics*. Int. Series Monogr. in Aeronautics and Astronautics, Pergamon.

Scorer, R. S. and F. H. Ludlam, 1953: Bubble theory of penetrative convection. *Q. J. R. Meteor. Soc.*, **79**, 94–103.

Shapiro, A. and Y. L. Kogan, 1994: On vortex formation in multicell convective clouds in a shear-free environment. *Atmos. Res.*, **33**, 125–136.

Telford, J. W., 1988: A theoretical solution to the motion of an atmospheric spherical vortex. *J. Atmos. Sci.*, **45**, 789–802.

Turner, J. S., 1962: The 'starting plume' in neutral surroundings. *J. Fluid Mech.*, **13**, 356–368.

— 1973: *Buoyancy effects in fluids*. Cambridge Monographs on Mechanics and applied mathematics, Syndics of the Cambridge University Press, Bentley House, 200 Euston Road, London NW I 2DB, 367 pp.

Vaillancourt, P. A., M. K. Yau, and W. W. Grabowski, 1997: Upshear and downshear evolution of cloud structure and spectral properties. *J. Atmos. Sci*, **54**, 1203–1217.

Woodward, B., 1959: The motion in and around isolated thermals. *Q. J. R. Meteor. Soc.*, **85**, 144–151.

Zhao, M. and P. H. Austin, 2005: Life cycle of numerically simulated shallow cumulus clouds. Part II: Mixing dynamics. *J. Atmos. Sci.*, **62**, 1291–1310, doi:10.1175/JAS3415.1.